ARMY RESEARCH LABORATORY

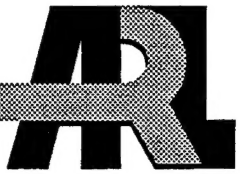

On a Pure Finite-Element-Based Methodology for Resin Transfer Mold (RTM) Filling Simulations

R. V. Mohan
N. D. Ngo
K. K. Tamma
UNIVERSITY OF MINNESOTA

K. D. Fickie
U.S. ARMY RESEARCH LABORATORY

ARL-TR-975 March 1996

NOTICES

Destroy this report when it is no longer needed. DO NOT return it to the originator.

Additional copies of this report may be obtained from the National Technical Information Service, U.S. Department of Commerce, 5285 Port Royal Road, Springfield, VA 22161.

The findings of this report are not to be construed as an official Department of the Army position, unless so designated by other authorized documents.

The use of trade names or manufacturers' names in this report does not constitute indorsement of any commercial product.

REPORT DOCUMENTATION PAGE

Form Approved
OMB No. 0704-0188

1. AGENCY USE ONLY *(Leave Blank)*	2. REPORT DATE	3. REPORT TYPE AND DATES COVERED
	March 1996	Final, June 1994–August 1995

4. TITLE AND SUBTITLE

On a Pure Finite-Element-Based Methodology for Resin Transfer Mold Filling Simulations

5. FUNDING NUMBERS

PR: 1L162618AH80

6. AUTHOR(S)

R. V. Mohan[a], N. D. Ngo[a], K. K. Tamma[a]
and K. D. Fickie

7. PERFORMING ORGANIZATION NAME(S) AND ADDRESS(ES)

U.S. Army Research Laboratory
ATTN: AMSRL-SC-SM
Aberdeen Proving Ground, MD 21005-5067

8. PERFORMING ORGANIZATION REPORT NUMBER

ARL-TR-975

9. SPONSORING / MONITORING AGENCY NAME(S) AND ADDRESS(ES)

10. SPONSORING / MONITORING AGENCY REPORT NUMBER

11. SUPPLEMENTARY NOTES

[a] Department of Mechanical Engineering, University of Minnesota,
111 Church Street S.E., Minneapolis, MN 55455

12a. DISTRIBUTION / AVAILABILITY STATEMENT

Approved for public release; distribution is unlimited.

12b. DISTRIBUTION CODE

13. ABSTRACT *(Maximum 200 words)*

A pure finite-element-based methodology for resin tranfer molding (RTM) process simulations is presented. The formulations are developed starting with the time-dependent mass conservation equation for the resin. Darcy's flow approximations are invoked for the velocity field forming a transient governing equation involving the pressure field and the resin saturation fill factor, which tracks the location of the resin front surface. Finite element approximations are then introduced for both the fill factor and the pressure field, and the resulting transient discrete equations are solved in an iterative manner for both the pressures and the fill factors tracking the progression of resin front in an Eulerian mold cavity. The formulation involves only a finite element Eulerian mesh discretization of the mold cavity and does not require specification of control volume regions and has no time increment restrictions that exist in traditional explicit finite element-control volume formulations. The present formulations accurately capture the physical transient nature of the mold-filling process while maintaining improved numerical and computational attributes. Mold-filling simulations involving various geometrically complex mold configurations are presented, demonstrating the applicability of the developments for manufacturing process simulations.

14. SUBJECT TERMS	15. NUMBER OF PAGES
molding techniques; composite structures; composite aircraft; manufacturing	36
	16. PRICE CODE

17. SECURITY CLASSIFICATION OF REPORT	18. SECURITY CLASSIFICATION OF THIS PAGE	19. SECURITY CLASSIFICATION OF ABSTRACT	20. LIMITATION OF ABSTRACT
Unclassified	Unclassified	Unclassified	UL

PAGE LEFT INTENTIONALLY BLANK

Acknowledgments

Special thanks are due to Mr. Phillip Harnden and Mr. Dale Shires of the U.S. Army Research Laboratory(ARL) for their graphics and visualization support. Their work was instrumental in model creation and visualization of the results. Thanks are also due to Dr. Ben Cummings, Dr. Tim Rohaly, Dr. Andrew Mark and Mr. Bill Mermagen of ARL for their support and encouragement during the course of this work.

The authors are very pleased to acknowledge support from Battelle/Army Research Laboratory. Partial support, in part from the Army High Performance Research Center (AHPCRC) at the University of Minnesota (on a contract from the U.S. Army Research Office) is also acknowledged. Additional support in the form of computer grants was furnished by the Minnesota Supercomputer Institute at the University of Minnesota, Minneapolis, MN.

PAGE LEFT INTENTIONALLY BLANK

Contents

PAGE LEFT INTENTIONALLY BLANK

List of Figures

List of Tables

PAGE LEFT INTENTIONALLY BLANK

1 Introduction

Resin transfer molding (RTM) is being increasingly employed in the manufacture of large components of fiber-reinforced composite materials. The process involves injection of resin into a mold cavity filled with fiber mat. Since good, close tolerances can be obtained by a good mold, this process is suited for manufacturing situations involving close tolerances.

Most of the present work in RTM simulations employs Eulerian fixed meshes modeling the mold cavity with a finite element-control volume approach and philosophy to track the flow field and filled regions of the mold [1-5]. In these finite element-control volume based approaches, a parameter called fill factor is associated with each node. Each node is associated with a control volume region, and the nodal fill factor indicates if the associated control volume region is empty or full. A fill factor of 1 corresponds to a filled region saturated with the resin, while a fill factor of 0 corresponds to an unfilled region. The resin flow front exists in control volume regions where the fill factor is between 0 and 1. The solution process involves solving for the pressure field based on both the continuity equation invoking Darcy's law and the fill factor. The filled regions and the fill factors are computed based on the actual flow rates and the control volumes associated with each node. This approach makes the mold-filling process to be regarded as a quasi-steady process, even though it is a transient process, assuming a steady-state condition at each time step. At each time step, the pressure distribution is computed based on both the boundary conditions and the fill factor condition. The velocity field, hence, the flow rate computed from the pressure field, is used to update the new front location, fill stage, and time of simulation. The selection of the time step increment for each of the quasi-steady state is based on the consideration that the time increment used allows only one control volume region to be completely filled. This restriction of the time increment ensures the stability of the quasi-steady state approximation and forms the so-called explicit filling methodology. In principle, three approaches are evident in the filling simulations based on Eulerian meshes, which includes the finite-element-control volume method and other related techniques such as the marker and cell (MAC) method and the volume of fluid (VOF) method.

Other techniques to determine the filled regions have been employed in analyzing the flow and filled regions in metal casting flow simulations [6]. The MAC technique combines the computational Eulerian mesh with a set of Lagrangian particles (the markers) representing the fluid configuration,

and moving through the Eulerian mesh according to the velocity vector field and defining where the fluid is located. In these metal casting flow simulations, the transient Navier-Stokes and continuity equations are solved for the velocity field. The VOF is another method that is commonly employed in mold flow simulation in metal castings[7-10]. In this, a factor, F, representing the fill factors associated with the node and the control volume region, is tracked and solved using a transport equation of the form:

$$\frac{\partial F}{\partial t} + \boldsymbol{u} \cdot \nabla F = 0. \tag{1}$$

The velocity field is again solved using the time-dependent Navier-Stokes equation and the continuity equation, and the factor F is between 0 and 1.

In considering the aforementioned approaches employed in the filling of mold cavities either in polymer-filling or casting applications, it is clear that, in addition to the flow field, a fill factor indicating the status of the region (filled or empty) is to be solved and determined. The explicit filling methodology, described earlier and used in finite element-control volume techniques for resin filling inside a porous mold cavity, involves only the continuity equation given by $\nabla \cdot \boldsymbol{u} = 0$, based on an incompressible resin and the velocity field approximated using Darcy's approximation. This necessitates the solution of the pressure field using the continuity equation and explicit determination of velocity fields and the flowrates based on the velocity field in each of the control volume regions defined for each node of the finite element mesh defined for the pressure field solution. This approach also restricts the incremental time employed in the time marching of the resin flow front.

It is to be noted that the objective of the mold-filling analysis is the conservation of resin mass at any instant of time and determination of its distribution inside a Eulerian mesh mold cavity. The fill factor implicitly defines the amount of resin present at any time inside a mold cavity and its distribution. In this report, an alternate form of the mass balance, or continuity equation, involving a time derivative of fill factor, to be determined is proposed. The velocity field is then approximated based on Darcy's law for flow through a porous, permeable medium. Finite element approximations for both the pressure field and the fill factor are introduced, thus providing a pure finite element methodology not involving the definition of the control volumes for both the pressure field and the fill factors. The resulting time-dependent system of equations are solved both for the pressure field and the fill factors defining the resin location inside a Eulerian mold cavity in an

iterative manner. The time-dependent system of equations can be solved employing any time step, and the pressure field and the filled regions at discrete time steps during the analysis are determined.

The developments are presented based on the following assumptions: 1) the polymer resin is incompressible; 2) the viscosity of the resin is taken to be constant and the filling is taken to be at isothermal conditions; 3) the flow is governed by Darcy's law and the Reynolds number is small to neglect the effect of inertial terms; and 4) the body forces and the gravity effects are not included. Though the developments are presented based on these assumptions, the present formulations can be easily extended to situations involving nonisothermal cases and where the body forces and gravity effects are involved.

The accuracy issues and computational advantages of the pure finite-element methodology proposed here are highlighted. Several numerical examples are presented to demonstrate the applicability of the method for polymer-filling simulations. Though the examples are presented in the context of thin mold configurations in general 3-D space, the developments are valid for general 1-, 2-, or 3-D mold-filling simulations and will be demonstrated in a subsequent report.

2 Pure Finite Element Methodology

Before presenting the pure finite element methodology for the solution of the pressure field and the fill factors, an alternate form of conservation mass equation is considered. This equation is based on resin mass conservation involving the time derivative of the fill factor.

2.1 Conservation of Resin Mass

As discussed earlier, the objective of the polymer resin mold-filling analysis is the conservation of the resin mass at any instant of time flowing through a porous mold cavity. The fill factor implicitly defines the amount of resin present inside the mold at any time and its distribution. Thus, considering a general Eulerian mold domain Ω with mass flux due to the incoming resin at the gates (as shown in Figure 1), at any instant of time, part of the mold cavity is filled with resin and the fill factor (Ψ) in the filled regions is greater than zero with the maximum value of fill factor (Ψ) being equal to one. In

unfilled regions, the resin fill factor (Ψ) is equal to zero. The mass of the resin inside the mold at any instant of time is then given by

$$\int_{\Omega} \rho \Psi d\Omega, \tag{2}$$

where ρ is the density of the polymer resin and the definition of Ψ considers only the mold cavity filled with resin. Since the mass conservation is maintained at any instant of time, the mass conservation equation or continuity equation for the resin at any instant of time [11, 12] can be written as (based on application of Reynolds transport equation)

$$\frac{\partial}{\partial t} \int_{\Omega} \rho \Psi d\Omega = - \int_{\partial\Omega} \rho \Psi \boldsymbol{u} \cdot \boldsymbol{n} \, d \, \partial\Omega. \tag{3}$$

For a constant density resin based on isothermal, incompressible conditions, the modified mass conservation equation for the resin can be written as

$$\frac{\partial}{\partial t} \int_{\Omega} \Psi d\Omega = - \int_{\partial\Omega} \Psi \boldsymbol{u} \cdot \boldsymbol{n} \, d \, \partial\Omega. \tag{4}$$

Eq. 4 forms the starting point for the development of the present numerical methodology.

2.2 Governing Equations

For polymer resin flow through porous media as in resin transfer molding flows, the velocity field is governed by Darcy's flow field approximation and is dependent on the permeability of the fiber preform and the resin viscosity and is given by

$$\boldsymbol{u} = -\frac{\boldsymbol{K}}{\mu} \bigtriangledown P, \tag{5}$$

where $\boldsymbol{K}$ is the permeability tensor of the fiber preform and is defined differently for 2-D and 3-D preform considerations. Using Darcy's approximation in the mass balance (Eq. 4) and employing the Greens theorem, the modified mass balance equation involving the fill factor and the pressure field is obtained and given as

$$\frac{\partial}{\partial t} \int_{\Omega} \Psi d\Omega = \int_{\Omega} \Psi \bigtriangledown \cdot \left(\frac{\boldsymbol{K}}{\mu} \bigtriangledown P \right) d\Omega. \tag{6}$$

It should be noted that the resin flow inside a mold cavity based on Darcy's flow approximation is a pressure-driven flow and the pressure gradients are negligible ($\nabla P \approx 0$) in unfilled and in regions that are partially filled where $0 \leq \Psi < 1$. In filled regions, $\Psi = 1$, and the variation in the fill factor are similar to those in the VOF method [7-9]. Hence, the modified mass balance equation governing the pressure-driven flow field is given by

$$\frac{\partial}{\partial t}\int_{\Omega} \Psi d\Omega = \int_{\Omega} \nabla \cdot \left(\frac{\boldsymbol{K}}{\mu} \nabla P\right) d\Omega. \tag{7}$$

This form of the mass balance equation involving the fill factor and the pressure field is the governing equation for the present finite element formulations. A differential form of the Eq. 7 is given by

$$\frac{\partial \Psi}{\partial t} = \nabla \cdot \left(\frac{\boldsymbol{K}}{\mu} \nabla P\right). \tag{8}$$

The boundary conditions for the mass balance equation can be stated as follows:

$$\begin{aligned}
\text{At mold surface} \quad & \frac{\partial P}{\partial n} = 0; \\
\text{At resin front} \quad & P = 0; \\
\text{At mold inlet} \quad & P = P_0 \quad \text{(prescribed pressure), or} \\
& u_n = -\frac{\boldsymbol{K}}{\mu}(\nabla P) = u_0 \quad \text{(prescribed flowrate);} \\
\text{At injection ports} \quad & \Psi(t \geq 0) = 1.0.
\end{aligned} \tag{9}$$

These forms of the mass balance equation involving the fill factor, pressure field, and the associated boundary conditions are discretized next using the finite element method.

2.3 Finite Element Discretization

To determine the pressure field and the resin saturation fill factors, the mold cavity is discretized and modeled using finite elements. For thin shell molds, 2-D elements with 2-D velocity field and 2-D permeabilities are employed. For thicker composite sections, 3-D velocity fields as given by Darcy's law and involving 3-D permeability tensors can be employed. Hence, the present

formulations are applicable for both thin and thick composites. We now discretize the mold geometry by discrete finite elements and introduce the finite element approximations for both the pressure and the fill factor. The introduction of finite element discretization for the fill factor $\Psi(0 \leq \Psi \leq 1)$ indicates that the fill factor has the same spatial variation as the pressure in each element.

$$\begin{aligned} P &= N_i P_i \\ \Psi &= N_i \Psi_i \end{aligned} \tag{10}$$

In the aforementioned equation, N_i are the spatial shape functions at each node of the finite element. P_i and Ψ_i are the nodal values of the pressure and the fill factors.

With these discretized approximations and invoking the traditional Galerkin-weighted residual formulation on the mass balance equation given by Eq. 7, we obtain

$$\begin{aligned} \frac{\partial}{\partial t}\left[\int_\Omega N_i N_j d\Omega\right]\Psi_i &= \left[-\int_\Omega \bigtriangledown N_i \boldsymbol{K} \bigtriangledown N_j d\Omega\right] P_i \\ &+ \int_{\partial\Omega}\Big(\bigtriangledown P \cdot \boldsymbol{n}\Big) N_i \, d\, \partial\Omega. \end{aligned} \tag{11}$$

This discretized system of equations can be written as

$$\boldsymbol{C}\dot{\boldsymbol{\Psi}} + \boldsymbol{K}\boldsymbol{P} = \boldsymbol{f}, \tag{12}$$

where

$$\boldsymbol{C} = \int_\Omega \boldsymbol{N}^T \boldsymbol{N} d\Omega, \tag{13}$$

$$\boldsymbol{K} = \int_\Omega \boldsymbol{B}^T \boldsymbol{K} \boldsymbol{B} d\Omega, \tag{14}$$

and

$$\boldsymbol{f} = \int_{\partial\Omega} (\bigtriangledown P \cdot \boldsymbol{n})\, \boldsymbol{N}^T \, d\, \partial\Omega, \tag{15}$$

where $\boldsymbol{B}$ defines the spatial derivatives of the shape functions employed for the finite element discretization.

Introducing the finite difference approximation for the time-derivative term in the Eq. 12, we have

$$\dot{\boldsymbol{\Psi}} = \frac{\boldsymbol{\Psi}^{n+1} - \boldsymbol{\Psi}^{n}}{\Delta t}. \tag{16}$$

The discretized finite element system is then given by

$$\boldsymbol{C}\left[\boldsymbol{\Psi}^{n+1} - \boldsymbol{\Psi}^{n}\right] + \Delta t \boldsymbol{K}\boldsymbol{P} = \Delta t \boldsymbol{f}. \tag{17}$$

For a lumped $\boldsymbol{C}$, the discretized equations can be written as

$$C_{ii}\Psi_i^{n+1} - C_{ii}\Psi_i^{n} + \Delta t K_{ij} P_j = \Delta t f_i. \tag{18}$$

Eq. 18 is a discrete equation for both the pressure and the fill factor Ψ and is solved in an iterative manner as described next.

2.4 Solution Strategy

The fill factors associated with the nodes and the pressure field are solved in an iterative manner based on the finite element discrete equations obtained (given by Eq. 18). The fill factors at the beginning of the simulation are known, and, at the nodes forming the injection ports, the fill factor is taken to be 1. The iterative procedure for solving the pressure field and the fill factor until mass conservation at each time step is preserved is described next [13].

1. At the beginning of each time step,

$$(\Psi_i)_m^{n+1} = (\Psi_i)^n, \tag{19}$$

   where m is the iteration number.

2. Apply the boundary conditions on $\boldsymbol{K}$.

   - Boundary conditions based on injection, vent pressures, and injection flow rates are applied.
   - Conditions based on the fill factor Ψ_i. These are applied at nodes where $\Psi_i < 1.0$.

3. Form

$$(g_i)_m = C_{ii}(\Psi_i)^n - C_{ii}(\Psi_i)_m^{n+1} + \Delta t f_i. \tag{20}$$

4. Solve $\hat{K}_{ij}(P_j)_m = (g_i)_m$, where $\hat{K}_{ij}$ is the modified $\boldsymbol{K}$ after the application of boundary conditions.

5. Update the nodal resin fraction field Ψ_i using the modified form of the discrete mass balance equation.

$$C_{ii}(\Psi_i)_{m+1}^{n+1} = C_{ii}\Psi_i^n - \Delta t K_{ij} P_j + \Delta t f_i. \tag{21}$$

   - Only a matrix vector product and vector additions are involved

6. Correct for under filling or over filling. Since Ψ can be either > 1 or < 0, a correction is to be made.

$$(\Psi_i)_{m+1}^{n+1} = max\left[0, min\left(1, (\Psi_i)_m^{n+1}\right)\right]. \tag{22}$$

7. Continue until convergence,

$$\left\| C_{ii}\{\Psi_i\}_{m+1}^{n+1} - C_{ii}\{\Psi\}_m^{n+1} \right\| \leq \epsilon. \tag{23}$$

8. Go to next time step.

2.5 Features and Advantages of the Present Methodology

Compared to the traditional explicit finite element-control volume methodology for simulation of resin transfer mold filling, the present methodology has significant physical, algorithmic, and computational advantages. These can be summarized as follows:

- The method is based on a time-dependent mass conservation of resin equation that solves for both the fill factors and the pressure fields, thus giving a direct transient problem formulation for mold filling. The method accurately captures the representative physics while maintaining improved numerical and computational attributes.

- The traditional finite element-control volume methodology requires identification and specification of the control volume regions associated with nodes of a given finite-element mesh discretization of mold cavity. This may become cumbersome when higher-order elements are involved. Further, the physical volumes associated with the control volume regions need to be computed. The present methodology only works with the finite-element mesh geometry, and the control volume regions associated with nodes need not be specified. Complex geometries can also be modeled using higher-order elements, and the finite-element mesh based on these higher-order elements can be made use of directly for subsequent structural stress simulations in a concurrent engineering environment.

- The traditional finite element-control volume methodology involves computation of the velocity fields, normals and bounding regions of the control volume for the computation of the flowrates, and subsequent computations of fill time to update the fill factors and movements of the flow fronts. The pure finite-element methodology involves only a matrix-vector product and vector additions in the updating of the fill factors and progression of the resin. This reduces the amount of computation and provides a significant computational advantage.

- The time increments on the finite element-control volume methodology are restricted so that no more than one complete control volume region is updated at each time increment. The present finite-element methodology does not have such a restriction and computes the position of the flow front at each of the selected discrete time intervals.

3 Numerical Examples

A variety of numerical examples are presented next to validate the present numerical developments and demonstrate the applicability to RTM simulations involving isothermal conditions. The present developments are valid and can be extended to nonisothermal conditions where the temperature, cure, and non-Newtonian effects of the viscosity are considered. The numerical examples involve 2-D triangular and quadrilateral element meshes involving complex 3-D mold cavities. The methodology is also directly ap-

plicable to higher-order elements and in full 3-D mold geometries involving 3-D elements [13-15].

3.1 Circular Plate With Constant Injection Pressure at the Center - Comparison with Analytical Solution

A circular plate with a hole of radius R_0 at the center forming the inlet gate of the mold is considered. The inner radius of the plate at radius R_0 is subjected to a constant pressure of P, and the flow is driven by this injection pressure. The cavity is of thickness H and the permeability of the fiber preform is taken to be K, with a porosity of fiber compaction denoted by Φ. Assuming a perfect complete radial flow, the time taken by the flow front to reach a radius R_f is given by

$$t = \frac{H\Phi}{KP} \int_{R_0}^{R_f} \frac{r ln \frac{r}{R_0}}{\int_0^H \frac{1}{\mu} dz} dr. \tag{24}$$

For constant viscosity μ_0, the time to reach a radius of R_f is given by

$$t = \frac{\mu_0 \Phi}{KP} \left\{ \frac{R^2}{2} ln \left(\frac{R_f}{R_0} \right) - \frac{R_f^2}{4} + \frac{R_0^2}{4} \right\}. \tag{25}$$

A circular plate model with the inner radius $R_0 = 0.0015$ m, with permeability $K = 44.0E - 12$ m^2, porosity $\Phi = 0.805$, viscosity $\mu_0 = 0.02$ poise, and subjected to an injection pressure of $69,000$ Pa is considered. The geometric mesh employed and the flow front contours are shown in Figure 2. The flow front, as computed by the analytical solution, is compared with the pure finite-element formulations and the explicit finite-element-control volume formulations as shown in Figure 3 (a). The comparison of flow front locations computed using different time step sizes employing the pure finite-element formulation are shown in Figure 3 (b). The numerical simulations are based on employing a 2-D quadrilateral mesh of 600 elements, with a 2-D isotropic permeability tensor, and an outer radius taken to be 0.1 m. The results compare well with the analytical solution, which is based on a perfect radial flow. The present formulations compute the flow front location at a given time with good accuracy, even when different time steps are employed to reach that stage. The total number of iterations taken to completely fill the mold and the average number of iterations per time step are

shown in Figure 3 (c) and Figure 3 (d). It should be noted as the time step size increases, the total number of iterations decreases, thus improving the computational performance.

3.2 Circular Plate With Constant Injection Flow Rate at the Center - Comparison with Analytical Pressure

The same circular plate as in the earlier case is considered. However, the plate is injected with a constant volumetric injection Q at the inlet radius, forming the inlet gate of the mold. Since the injection is at a constant flow rate, the injection pressure varies with time as the mold gets filled and provides a comparison of the simulated injection pressures with an analytical solution. An expression for the injection pressure and the radial location of the flow front is available and is used here. For this case, the front radius location $R_f(t)$ and the injection pressure P_0 at time t are given by

$$R_f(t) = \Big[\frac{Qt}{\pi\phi H} + R_0^2\Big]^{\frac{1}{2}}$$

and

$$P_0 = \frac{\mu Q}{2\pi K H} log \frac{R_f(t)}{R_0}. \tag{26}$$

The mesh and the physical properties of the fiber preform and the resin are the same as in the previous example. The flow rate Q is taken to be $2.36e-04\frac{m^3}{s}$. The flow front contours based on the present formulations with a time step size of 1.0 sec are shown in Figure 4. The flow front location as computed by the analytical solution is compared with the pure finite element formulation and the explicit finite element-control volume formulations as shown in Figure 5 (a). The location of flow fronts computed using different time step sizes employing the present formulations and the analytical solution are shown in Figure 5 (b). The variation of the total number of iterations and the average number of iterations based on time steps employed are shown in Figures 5 (c) and 5 (d). Being a constant flow rate injection, the injection pressure changes with time and the comparison of the injection pressure with time for the pure finite element formulation and the explicit finite element-control volume formulation are shown in Figure 6 (a). The

injection pressure comparisons with different time step sizes employed in the present formulations as compared with the analytical solution are shown in Figure 6 (b). The present formulations compute the given flow front location at a given time with good accuracy even when different time steps are employed to reach that stage.

3.3 Flow Fronts Advancement and Time Step Sizes

In the previous two examples, the flow front locations employing the different time step sizes and the pure finite element methodology are shown in Figure 3 (b) for the case of constant injection pressure at the inner radius and in Figure 5 (b) for the case of constant flow rate injection at the inlet radius. The time data for these figures were originally obtained by determining the time step interval at which the node locations along a certain radial direction got filled. The resolution of the time and the front location with this strategy depends on the time step size and only indicates that a given node location is completely filled at the end of a certain discrete time step, while the node physically could be filled between two discrete time steps employed in the analysis. Hence the comparison with the analytical solution shown earlier indicated that the flow front location accuracy varies with time step size. However, during the analysis, the computed time for complete filling remained the same even when employing larger time step sizes.

Numerical experiments involving analysis up to certain intermediate times also indicated that the filled and partially filled regions up to that time were the same (within the bounds of numerical errors) after the satisfaction of mass conservation up to that time. This clearly suggests that the predicted location of the flow fronts employing the present finite element methodology are independent of the time step size. It also suggests that the location of the flow front was not correctly resolved with the strategy employed earlier. In the two example cases involving a radial flow, the location of the front can be resolved based on the volume filled, as indicated by the fill factors obtained using different time step sizes used to reach that time level. An alternate way of resolving the flow front location at a given time step for radial flow is described next.

Consider the computed nodal fill factors at any instant of time t be F_I. This time instant can be reached employing different time step sizes and the

filled volume of the resin $V(t)$ at that instant is given by

$$V(t) = F_i C_{ii} \tag{27}$$

Let R be the radial location of the resin front at that time t. For the case of radial flow, we then have

$$\pi H(R^2 - R_0^2) = V(t) \tag{28}$$

from which the radial front location at any instant of time can be computed based on mass balance. The radial front locations employing the above strategy with different time step sizes are as shown in Figure 7 (a) for the case of constant inlet injection pressure and Figure 7 (b) for the case of constant inlet injection flow rate. From the two figures, it is clear that the flow front location does not depend on the time step size employed. The computed resin front advancement and impregnated region at any given time remains the same irrespective of the time step size employed to reach that stage, though, higher flow front progression resolution can be obtained with smaller time step sizes.

3.4 Circular Plate With an Eccentric Injection Gate

One of the advantages of the pure finite-element formulations is its computational efficiency. Traditional explicit finite element-control volume methodologies currently employed in the resin transfer molding simulations require computation of the velocity field and the flow rates and restriction of time step increment sizes based on the condition that only a single control volume region is filled at each time step. However, the present formulations do not involve these computations and, hence, are computationally efficient. In the study of the earlier two examples in which the flow is radial and with the mesh employing quadrilateral elements having a good radial symmetry, we found that the computational time for the traditional explicit finite element-control volume methodology and the present formulations were nearly identical. This can be attributed to the fact that the previous two examples with perfect radial symmetry allowed for the simultaneous filling of a row of control volumes in the explicit finite element-control volume methodology. Thus, the nearly equal times are attributed to this geometry and flow symmetry. As a test, we consider for this example the same circular plate geometry with the injection gate not at the center, but at an eccentricity to the plate geometry.

The flow is not radially symmetric in this case, and the mesh is also not radially symmetric. This being the case, the computational advantages of the present developments for the RTM simulations are clearly seen from Table 1.

From Table 1 and the comparisons shown for significantly larger practical examples shown later, the computational advantage of the present formulations is clearly evident. The total number of iterations, which is an indication of computational load, is also shown and compared with the explicit finite-element-control volume methodology in Table 1. The mesh geometry and the flow front contours based on a time step size $\Delta t = 1.0s$ are shown in Figure 8.

3.5 Risk Reduction Box

A complex 3-D risk reduction box geometry manufactured by the RTM process is considered. Since the production and tooling costs are expensive for the RTM process, manufacturing simulations are necessary to avoid costly trial runs. With the presence of corners and edges, the fiber preform permeability varies in those regions. Simulation tools should take into account these variations in the permeability variations. The fill time and pressure information and the study of the flow front progression with different injection conditions help in optimization of the mold and in process optimization to manufacture parts without any dry spots and within the residence life of the resin to allow for complete filling.

From a computational perspective, the considered mold geometry with geometric and multiple material regions provides a base to study the computational efficiency of the present method. A large finite-element mesh consisting of 4,380 nodes and 8,670 elements is considered. The mold is injected along the top edges of the risk reduction box geometry. The mesh geometry and the flow fill contours showing the fill pattern are shown in Figure 9. Isotropic permeabilities of 1.0075957e-10 m^2 in the flat regions and corner permeabilities, which are higher in magnitude by 10-100 times, were used for the simulations. The fill contours are representative of actual conditions and an examination of a representative box manufactured by the RTM process. The computational time and the iteration count of the pure finite element methodology for different time step sizes are compared with the traditional finite element-control volume methodology as shown in Table 2.

3.6 Crew Capsule of Composite Armored Vehicle (CAV)

A large finite element model representing the crew capsule of a composite armored vehicle (CAV) is considered in this analysis. The finite-element model employed has 12,187 nodes and 24,240 triangular elements. Two views of the mesh geometry are shown in Figure 10. For a demonstrative injection location, the fill pattern contours are shown in Figure 11. The explicit finite element-control volume methodology involved a total number of 11,007 iterations, and the total number of iterations for the present methodology are significantly smaller, as shown in Table 3. The computational time of the pure finite element methodology for different time step sizes is compared with the explicit finite element-control volume methodology, as shown in Table 3.

4 Concluding Remarks

This report describes a pure finite element-based methodology for RTM filling simulations. The pure finite-element methodology has significant computational advantages compared to the traditional explicit finite element-control volume approaches. For the mold filling simulation of the crew capsule with 12,187 nodes and 24,240 elements, the pure finite-element-based methodology is faster by a factor of nearly 30, even with a time step size of 1.0 sec. More importantly, the proposed methodology inherits good accuracy to accurately capture the representative physics while maintaining improved numerical and computational attributes. The present methodology has no time step increment restrictions as in the traditional explicit finite element-control volume methodology and works only with a finite element mesh geometry, making its application direct and easier. The mold filling simulation examples illustrate the practical applicability of the method in manufacturing simulation situations. The developments are valid and can be easily extended to other situations involving pressure-driven filling and porous media flows.

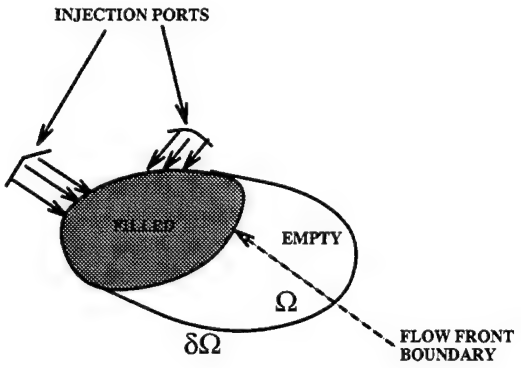

Figure 1: General partially filled mold cavity

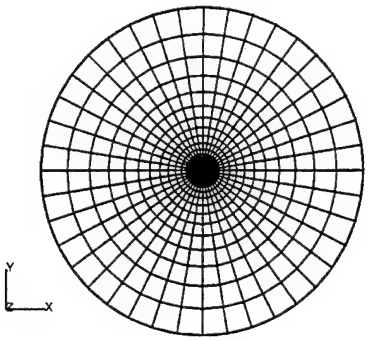

(a) Mold plate mesh geometry

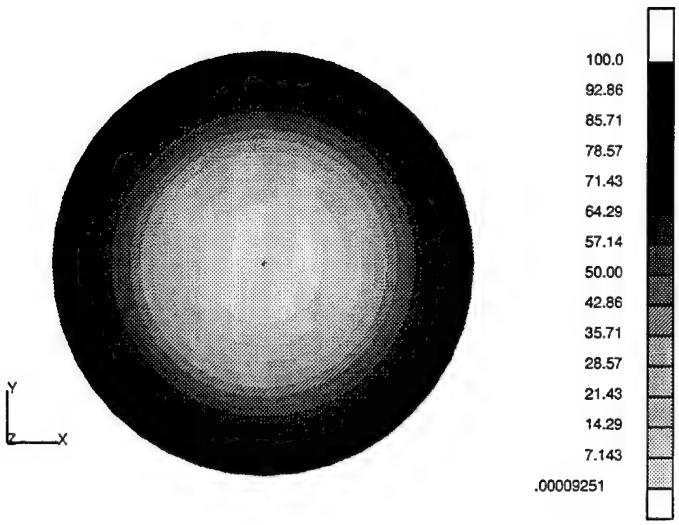

(b) Fill contours in the mold

Figure 2: Circular plate geometry: constant pressure injection

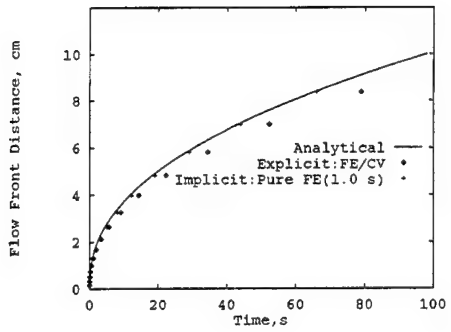

(a) Comparison with explicit: FE/CV

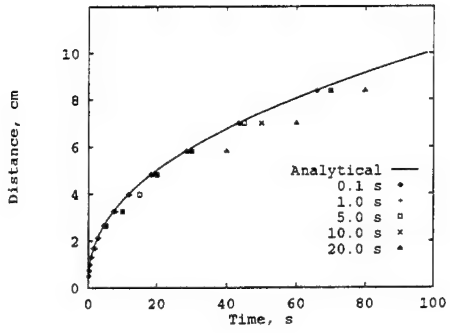

(b) Pure FE comparisons

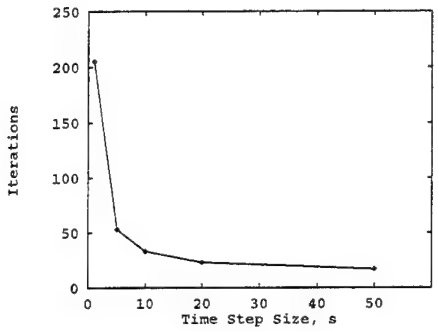

(c) Pure FE: total number of iterations

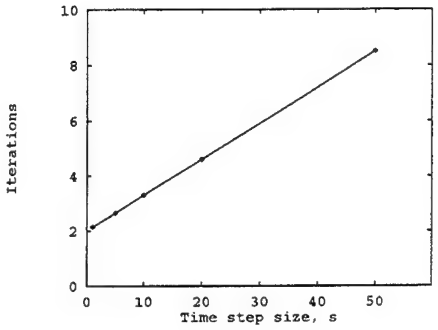

(d) Pure FE: ave. iterations/time step

Figure 3: Circular plate mold-flow front and iteration comparisons: constant pressure injection

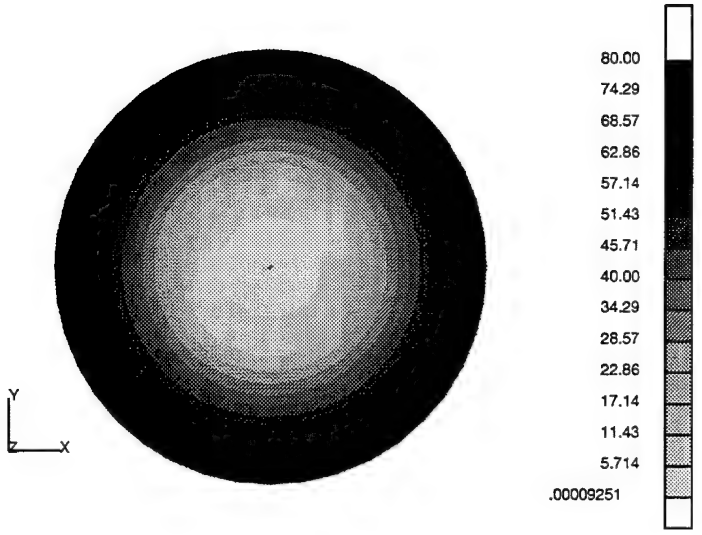

Figure 4: Flow fill contours: constant flowrate injection

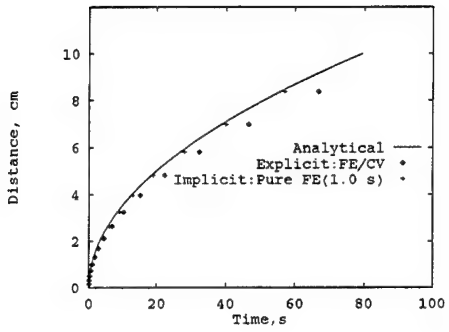

(a) Comparison with explicit: FE/CV

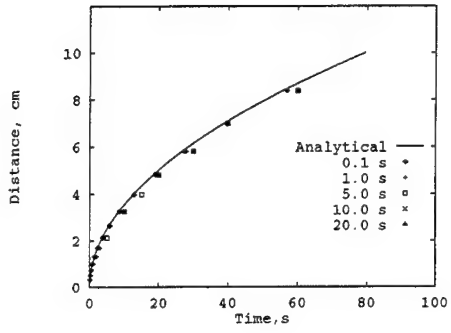

(b) Pure FE comparisons

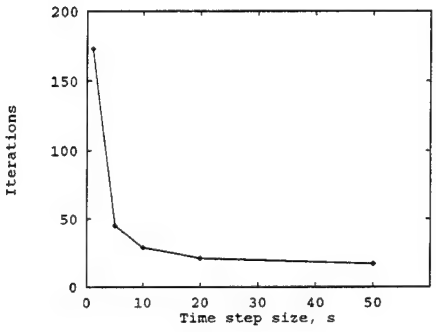

(c) Pure FE: total number of iterations

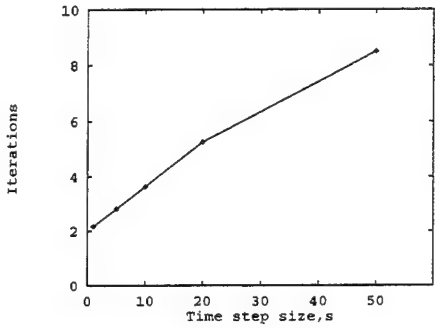

(d) Pure FE: ave. iterations/time step

Figure 5: Circular plate mold-flow front and iteration comparisons: constant flowrate injection

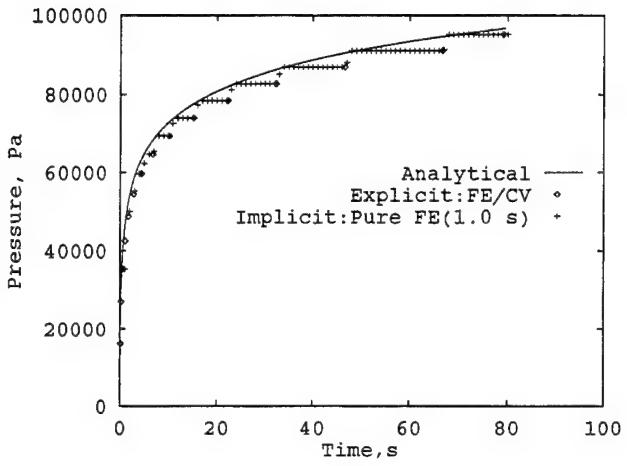

(a) Comparison with explicit: FE/CV

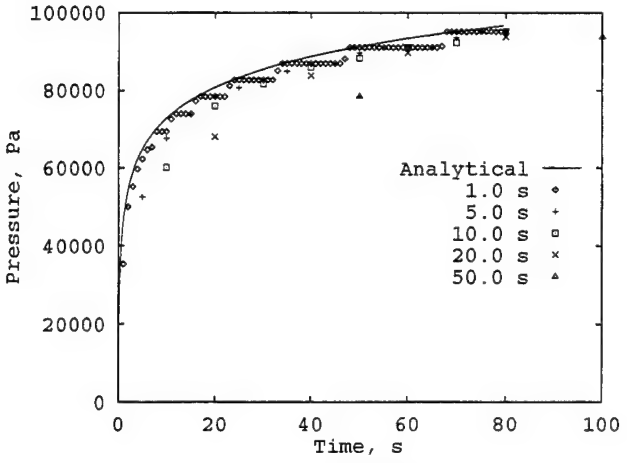

(b) Pure FE comparisons

Figure 6: Comparison of injection pressures: constant flowrate injection

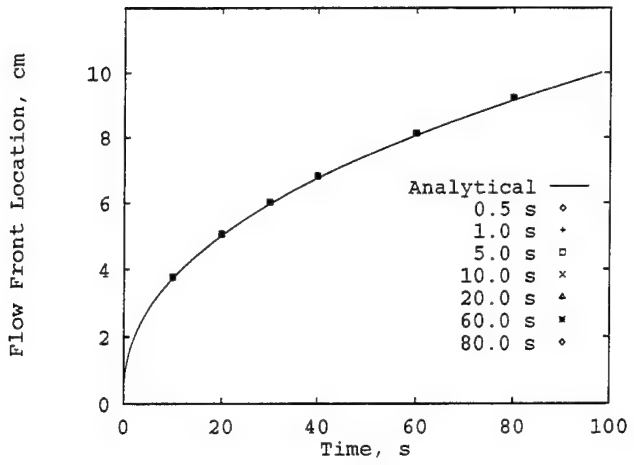

(a) Constant inlet injection pressure case

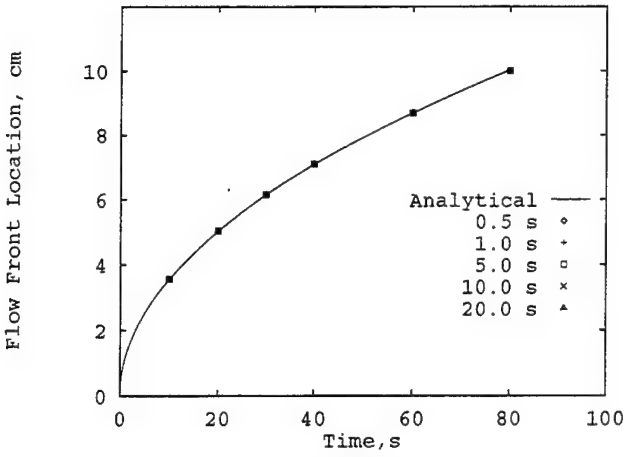

(b) Constant inlet injection flow rate case

Figure 7: Comparison of flow fronts

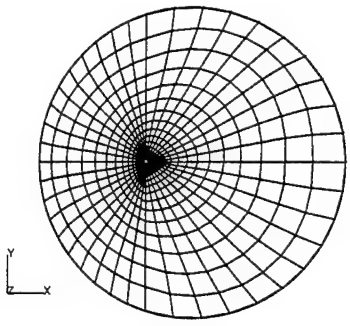

(a) Mold plate mesh geometry

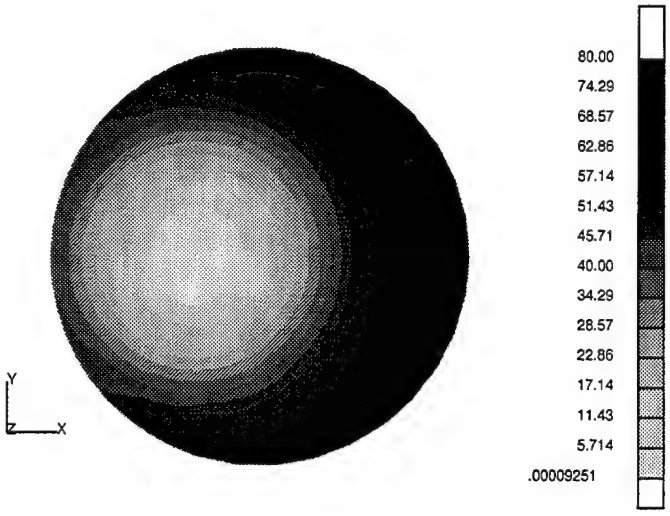

(b) Fill contours in the mold

Figure 8: Circular plate: eccentric injection gates-constant flowrate injection

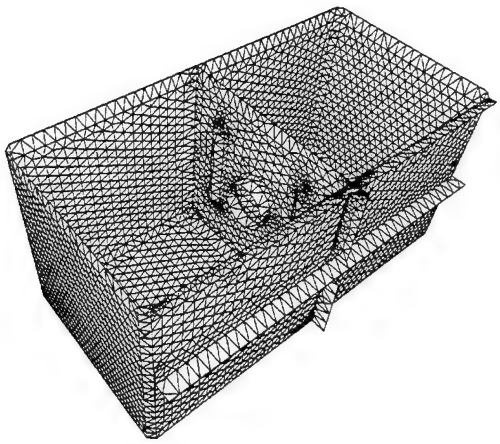

(a) mesh geometry

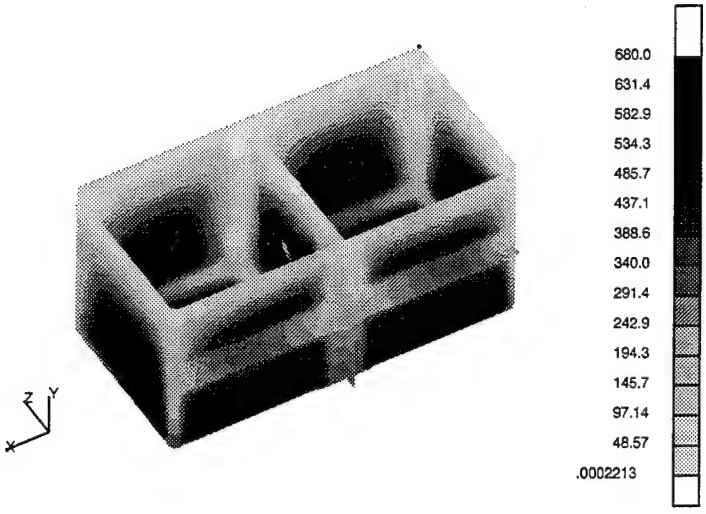

(b) Fill contours in the mold

Figure 9: Risk reduction box mold filling simulation

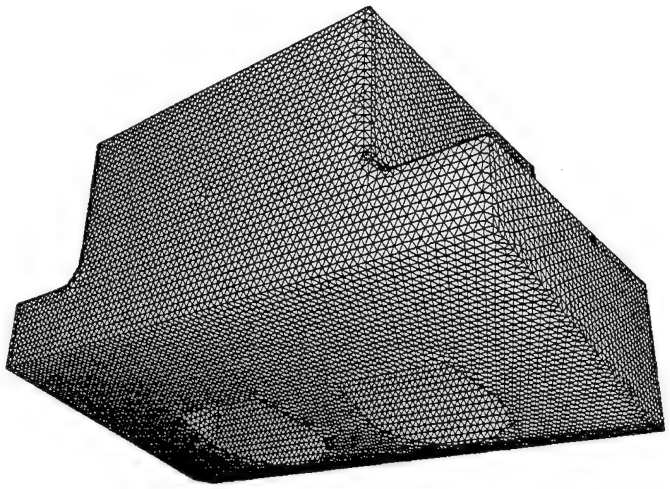

(a) view 1

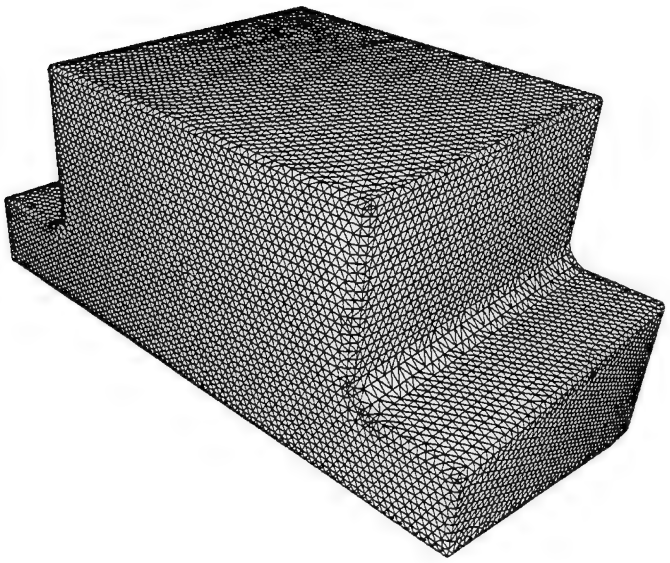

(b) view 2

Figure 10: Crew capsule: mesh geometry

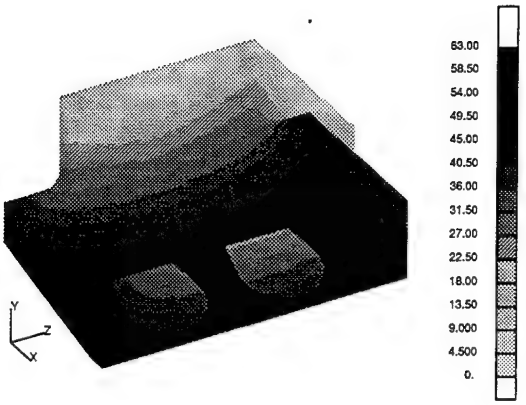

(a) Fill contours - view 1

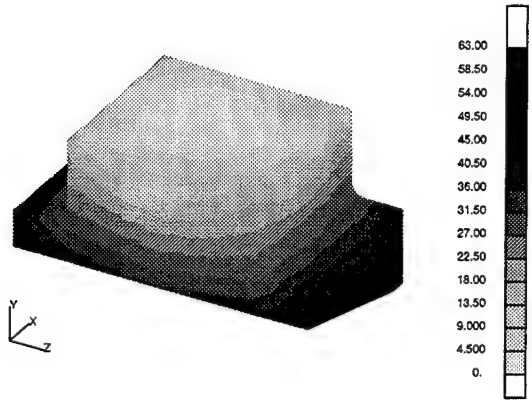

(b) Fill contours - view 2

Figure 11: Crew capsule: fill contours

Table 1: Comparison of computational times:circular plate with an eccentric injection gate

Method	Computational time[a]	Total no. of iterations
Explicit FE-CV	21.96	551
Pure FE		
$\Delta t = 1.0$ sec	9.27	266
$\Delta t = 5.0$ sec	2.80	76
$\Delta t = 10.0$ sec	1.77	46
$\Delta t = 20.0$ sec	1.41	32
$\Delta t = 50.0$ sec	1.00	23

[a]Relative to the actual computational time corresponding to $\Delta t =$ 50.0 sec.

Table 2: Comparison of computational times:risk reduction box

Method	Computational time[b]	Total no. of iterations
Explicit FE-CV	43.86	3808
Pure FE		
$\Delta t = 5.0$ sec	7.02	557
$\Delta t = 10.0$ sec	4.23	329
$\Delta t = 20.0$ sec	2.74	202
$\Delta t = 40.0$ sec	1.76	136
$\Delta t = 85.0$ sec	1.37	97
$\Delta t = 170.0$ sec	1.045	74
$\Delta t = 340.0$ sec	1.0	59

[b]Relative to the actual computational time corresponding to $\Delta t =$ 340.0 sec.

Table 3: Comparison of computational times:crew capsule of CAV

Method	Computational time[c]	Total no. of iterations
Explicit FE-CV	104.97	11,007
Pure FE		
$\Delta t = 1.0$ sec	3.52	350
$\Delta t = 3.0$ sec	1.87	176
$\Delta t = 7.0$ sec	1.37	124
$\Delta t = 16.0$ sec	1.11	93
$\Delta t = 32.0$ sec	1.00	83

[c] Relative to the actual computational time corresponding to $\Delta t = 32.0$ sec.

References

[1] C. A. Fracchia. Numerical simulation of resin transfer mold filling. Master's thesis, University of Illinois at Urbana-Champaign, IL, 1990.

[2] C. L. Tucker, C. A. Fracchia, and J. Castro. A finite element/control volume simulation of resin transfer mold filling. In *Proc. of the American Society For Composites, 4th technical conference*, Lancaster, PA, 1957.

[3] M. V. Bruschke and S. G. Advani. A numerical simulation of the resin transfer mold filling process. In *ANTEC*, 1990.

[4] M. V. Bruschke and S. G. Advani. A finite element/control volume approach to mold filling in anisotropic porous media. *Poly. Comp*, 11(6), 1990.

[5] F. Trouchu, R. Gauvin, and D. M. Gao. Numerical analysis of the resin transfer molding process by the finite element method. *Advances in Polymer Technology*, 12(4):329–342, 1993.

[6] Weng-Sing Hwang and R. A. Stoehr. Molten metal flow pattern prediction for complete solidification analysis of near net shape castings. *Materials Science and Technology*, 4:240–250, March 1988.

[7] G. Dhatt, D. M. Gao, and A. Ben Cheikh. A finite element simulation of mold flow in moulds. *Int. J. Num. Meth. Engg*, 30:821–831, 1990.

[8] C. W. Hirt and B. D. Nichols. Volume Of Fluid method for the dynamics of free boundaries. *J. Computational Physics*, 39:201–225, 1981.

[9] R. A. Stoehr and C. Wang. Coupled heat transfer and fluid flow in the filling of castings. *AFS Transactions*, pages 733–740, 1988.

[10] C. R. Swaminathan and V. R. Voller. A time-implicit filling algorithm. *Applied Math. Modelling*, 18:101–108, February 1994.

[11] Irving H. Shames. *Mechanics of Fluids.* McGraw-Hill Book Company, New York, 1982.

[12] I. G. Currie. *Fundamental Mechanics of Fluids.* McGraw-Hill Book Company, New York, 1974.

[13] V. R. Voller and S. Peng. An algorithm for analysis of filling in polymer filling. *Polym. Eng. Sci*, in press, 1995.

[14] R. V. Mohan, N. D. Ngo, K. K. Tamma, and K. D. Fickie. Three-dimensional developments for thick RTM composites. *J. Polymer Science and Engineering*, submitted, 1995.

[15] R. V. Mohan, N. D. Ngo, K. K. Tamma, and K. D. Fickie. Three-dimensional resin transfer molding process simulations: computational developments and issues. In *U.S. Congress in Computational Mechanics*, Dallas, TX, June 1995.

[16] K. Tamma et al. An overview of recent developments and advances in resin transfer molding of thin/thick composite structures. ARO Report, University of Minnesota, MN, October 1994.

NO. OF COPIES	ORGANIZATION
2	DEFENSE TECHNICAL INFO CTR ATTN DTIC DDA 8725 JOHN J KINGMAN RD STE 0944 FT BELVOIR VA 22060-6218
1	DIRECTOR US ARMY RESEARCH LAB ATTN AMSRL OP SD TA 2800 POWDER MILL RD ADELPHI MD 20783-1145
3	DIRECTOR US ARMY RESEARCH LAB ATTN AMSRL OP SD TL 2800 POWDER MILL RD ADELPHI MD 20783-1145
1	DIRECTOR US ARMY RESEARCH LAB ATTN AMSRL OP SD TP 2800 POWDER MILL RD ADELPHI MD 20783-1145
	ABERDEEN PROVING GROUND
5	DIR USARL ATTN AMSRL OP AP L (305)

NO. OF COPIES	ORGANIZATION
36	ABERDEEN PROVING GROUND

DIR USARL
ATTN AMSRL SC
N. BOYER
R. LODER
W. MERMAGEN
AMSRL SC C
C. NIETUBICZ
AMSRL SC CC
P. DYKSTRA
J. GROSH
T. KENDALL
C. ZOLTANI
AMSRL SC CN
D. TOWSON
AMSRL SC S
M. BIEGA
B. BODT
A. MARK
M. TAYLOR
AMSRL SC SM
R. MOHAN
D. SHIRES
AMSRL SC SS
C. HANSEN
E. HEILMAN
T. PURNELL
K. SMITH
M. THOMAS
V. TO
AMSRL SC SA
J. WALL
AMSRL SC A
R. ROSEN
AMSRL SC I
E. BAUR
J. GANTT
M. HIRSCHBERG
AMSRL SC II
J. DUMER
R. HELFMAN
AMSRL IS TP
B. BROOME
S. CHAMBERLAIN
B. COOPER
A. DOWNS
D. GWYN
G. HARTWIG
M. MARKOWSKI

USER EVALUATION SHEET/CHANGE OF ADDRESS

This Laboratory undertakes a continuing effort to improve the quality of the reports it publishes. Your comments/answers to the items/questions below will aid us in our efforts.

1. ARL Report Number ARL-TR-975 Date of Report March 1996

2. Date Report Received _____

3. Does this report satisfy a need? (Comment on purpose, related project, or other area of interest for which the report will be used.) _____

4. Specifically, how is the report being used? (Information source, design data, procedure, source of ideas, etc.) _____

5. Has the information in this report led to any quantitative savings as far as man-hours or dollars saved, operating costs avoided, or efficiencies achieved, etc? If so, please elaborate. _____

6. General Comments. What do you think should be changed to improve future reports? (Indicate changes to organization, technical content, format, etc.) _____

CURRENT ADDRESS

_____
Organization

_____
Name

_____
Street or P.O. Box No.

_____
City, State, Zip Code

7. If indicating a Change of Address or Address Correction, please provide the Current or Correct address above and the Old or Incorrect address below.

OLD ADDRESS

_____
Organization

_____
Name

_____
Street or P.O. Box No.

_____
City, State, Zip Code

(Remove this sheet, fold as indicated, tape closed, and mail.)
(DO NOT STAPLE)

DEPARTMENT OF THE ARMY

OFFICIAL BUSINESS

NO POSTAGE
NECESSARY
IF MAILED
IN THE
UNITED STATES

BUSINESS REPLY MAIL
FIRST CLASS PERMIT NO 0001,APG,MD

POSTAGE WILL BE PAID BY ADDRESSEE

DIRECTOR
U.S. ARMY RESEARCH LABORATORY
ATTN: AMSRL-SC-SM
ABERDEEN PROVING GROUND, MD 21005-5067